

RESEARCH ARTICLE | JUNE 17 2025

Point defect luminescence associated with stacking faults in magnesium doped zincblende GaN

Xiuyuan Xu ; Martin Frentrup ; Gunnar Kusch ; Ruiying Shu ; Christina Hofer; Paul A. J. Bagot ; Michael P. Moody; Menno J. Kappers ; David J. Wallis ; Rachel A. Oliver 



J. Appl. Phys. 137, 235301 (2025)

<https://doi.org/10.1063/5.0274599>



View
Online



Export
Citation

Point defect luminescence associated with stacking faults in magnesium doped zincblende GaN

Cite as: J. Appl. Phys. **137**, 235301 (2025); doi: [10.1063/5.0274599](https://doi.org/10.1063/5.0274599)

Submitted: 7 April 2025 · Accepted: 29 May 2025 ·

Published Online: 17 June 2025



Xiuyuan Xu,^{1,a)}  Martin Frentrup,¹  Gunnar Kusch,¹  Ruiying Shu,²  Christina Hofer,² Paul A. J. Bagot,² 
Michael P. Moody,² Menno J. Kappers,¹  David J. Wallis,^{1,3}  and Rachel A. Oliver¹ 

AFFILIATIONS

¹Department of Materials Science and Metallurgy, University of Cambridge, 27 Charles Babbage Rd, Cambridge CB3 0FS, United Kingdom

²Department of Materials, University of Oxford, Parks Road, Oxford OX1 3PH, United Kingdom

³Centre for High Frequency Engineering, University of Cardiff, 5 The Parade, Newport Road, Cardiff CF24 3AA, United Kingdom

^{a)}Author to whom correspondence should be addressed: xx838@cam.ac.uk

ABSTRACT

The luminescence characteristics and the relation between the distribution of impurities and stacking faults (SFs) in Mg-doped zincblende gallium nitride (zb-GaN:Mg) have been investigated by cathodoluminescence (CL) and atom probe tomography (APT). Four peaks have been identified in the CL emission spectrum, and the possible related recombination mechanisms have been proposed. The main peak at 3.23 eV is associated with excitonic transitions, while the other three, having lower energies at about 3.15, 3.02, and 2.92 eV, respectively, are related to donor-to-acceptor (DAP) transitions involving different acceptor energy levels. These DAP peaks were significantly more intense on or close to SFs compared to the surrounding defect-free material, indicating an enrichment of point defects near SFs. This finding was supported by APT measurements, where Mg showed a tendency to segregate toward SFs in zb-GaN.

© 2025 Author(s). All article content, except where otherwise noted, is licensed under a Creative Commons Attribution (CC BY) license (<https://creativecommons.org/licenses/by/4.0/>). <https://doi.org/10.1063/5.0274599>

I. INTRODUCTION

Gallium nitride (GaN) and its alloys have been widely used for lighting after the revolutionary development of high-efficiency blue light-emitting diodes (LEDs).^{1,2} These blue LEDs are conventionally based on wurtzite (wz) InGaN/GaN multiple-quantum wells (MQWs) grown in the hexagonal phase on the polar c-plane. However, such blue LEDs suffer from an efficiency droop with increasing local current density, required in small LEDs with high brightness for display applications.³ Furthermore, spontaneous and piezoelectric polarization fields along the c-axis will reduce the radiative recombination rates in QWs, which leads to reduced internal quantum efficiency of green wz-InGaN-based LEDs in comparison with blue LEDs.⁴ Currently, the efficiency of these green LEDs is only half that of blue InGaN and red phosphide based LEDs, a phenomenon known as the “green gap” problem.⁵ Zincblende GaN (zb-GaN) grown in the (001) orientation offers an

alternative route, as it is free from polarization fields due to its high structural symmetry and, for which, a significantly smaller efficiency droop is expected compared to wz-GaN-based LEDs.⁶ However, zb-GaN suffers from the high density of {111}-type stacking faults (SFs), which are the dominant extended planar defects in zb-GaN.^{7,8} SFs are detrimental to the optical properties of zb-GaN, possibly because these inclined planar wz-like defects might be susceptible to the incorporation of point defects during growth, similar to the SFs in semipolar wz-GaN.⁹ These point defects may give rise to non-radiative recombination near SFs.^{9–11} Theoretical work has shown the possibility of point defect segregation at SFs. For example, Schmidt *et al.* suggested the segregation of Mg impurities toward SFs in zb-GaN:Mg, where Mg impurities can achieve the lowest equilibrium energy by substituting onto Ga-sites in the plane of the SF.¹² Meanwhile, spectroscopic studies have shown that several peaks in the photoluminescence (PL) spectra of

24 June 2025 15:00:39

zb-GaN:Mg may relate to transitions into Mg acceptor states.^{13–15} These characteristic transitions provide an opportunity to investigate the distribution and potential Mg accumulation at or near SFs via the spatial variation in the Mg-related luminescence signatures.

Scanning electron microscopy (SEM) and cathodoluminescence (CL) are the ideal methods for such an investigation. In previous studies, SEM-CL has been used to map the distribution of SFs across a zb-GaN epilayer and zb-InGaN single quantum well and to investigate their optical properties. In the earlier stage, most works focused on the luminescence peaks of SFs in the CL spectra and their underlying recombination mechanisms and investigated the role of other defects in the vicinity of SFs, such as point defects.^{9,16} While the specific signatures in the CL spectra provide evidence for the existence of certain defects, they do not provide insight into the luminescence of specific SF-related features near the surface. To overcome this issue, hyperspectral CL maps have been used in the past, to correlate the light emission with specific SF-related features seen in secondary electron (SE) images.^{9,17} Similarly, the distribution of impurities can be investigated by analyzing the defect-related luminescence features from CL maps and correlating them with the SF-related features in the corresponding SE images. Furthermore, Kumar *et al.*^{18,19} have performed atom probe tomography (APT) to measure the Mg concentration near the dislocations in Mg-implanted wz-GaN, and investigated the influences of annealing temperature on Mg clustering near these defects. Their research suggests Mg segregation toward the dislocations in wz-GaN, and supports the idea that APT can be used to map the impurity distribution at the defects in zb-GaN.

In this study, we focus on the correlation of the distributions of Mg impurities and SFs in zb-GaN:Mg by CL and APT, addressing the potential segregation of Mg impurities toward SFs in the material. CL was used to identify the luminescence features related to impurities and to map the spatial distribution of these features. This was supported by APT measurements, which were used to investigate the distribution of elements at SF locations.

II. EXPERIMENTAL METHODS

The as-grown zb-GaN:Mg sample investigated in this study was grown on a 3C-SiC/Si (001) pseudo-substrate by metal organic vapor-phase epitaxy (MOVPE) in a $6 \times 2''$ Aixtron close-coupled showerhead reactor. A 4° miscut along $[1 \ -1 \ 0]$ was present in the substrate to avoid the formation of antiphase domains.²⁰ After the initial growth of an approximately 45 nm-thick nucleation layer at standard growth conditions, a 2300 nm-thick zb-GaN:Mg epilayer was grown at 100 Torr, 890 °C, and a V/III ratio of 76, following the previous optimization studies.²¹ After growth, the sample was cooled down to room temperature without additional *in situ* annealing or postgrowth activation of Mg. A control experiment at room temperature has also shown little or no Mg activation under the irradiation of the electron beam during CL measurements. Secondary-ion mass spectrometry analysis of a similarly grown sample shows a concentration of $3 \times 10^{19} \text{ cm}^{-3}$ magnesium, $4 \times 10^{17} \text{ cm}^{-3}$ oxygen, $9 \times 10^{18} \text{ cm}^{-3}$ hydrogen, and $4 \times 10^{19} \text{ cm}^{-3}$ carbon.

In this work, the CL maps and SE images were acquired using an Attolight Allalin 4027 Chronos SEM-CL system, equipped with

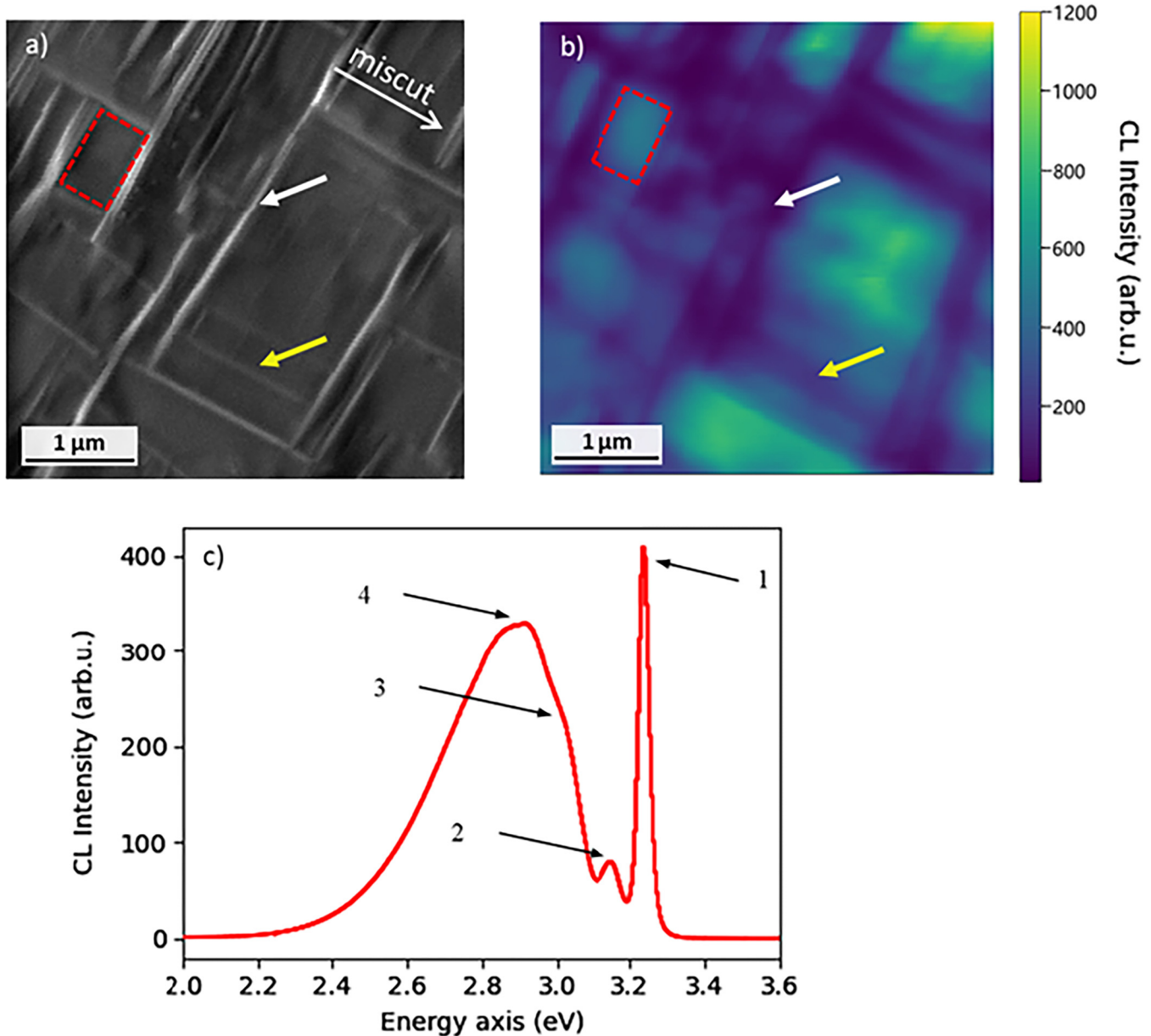
a cryostat. All measurements were performed at 80 K, with 5 keV beam energy, resulting in an interaction volume of about 90 nm, 1.25 nA probe current, 50 μm aperture size, and a 150 l/mm grating blazed at 500 nm. The pixel dwell time was 100 ms, and the size of the CL maps and SE images is $4.26 \times 4.26 \mu\text{m}^2$. All data were analyzed using the python-based LumiSpy package.²² The samples for APT were prepared in a Zeiss Crossbeam 540 Analytical FIB-SEM system. Prior to preparation, a protective chromium layer was deposited on the sample via Leica EM ACE600 to safeguard the surface during processing. APT samples were extracted using the standard lift-out approach.²³ To minimize the milling damage, the final stage of polishing to reach the near-surface layer of interest was carried out at 2 kV and 10 pA. APT measurements were conducted at 50 K in CAMECA LEAP5000-XS in the laser mode with a laser energy of 10 pJ per pulse. The APT datasets were analyzed using the commercial software packages IVAS 6.3 and AP Suite 6.1.

III. RESULTS AND DISCUSSION

The SE image in Fig. 1(a) shows the typical surface morphology of the zb-GaN:Mg sample and Fig. 1(b) shows the corresponding panchromatic CL map of the same area. Three different surface features can be identified from the SE image: flat rectangular areas, elongated surface features, and pale stripes, which are marked by a red dashed rectangle, a white arrow, and a yellow arrow, respectively. The flat rectangular features are free from pale stripes and correspond to the high-intensity bright patches in the panchromatic CL map (as indicated by the red dashed rectangle in the CL map). The elongated surface features align parallel to and perpendicular to the sample miscut and correspond to the lines of low emission intensity in the CL image. For example, in the CL map, a white arrow points to a dark line with low emission intensity which corresponds to a surface feature perpendicular to the miscut, as indicated by the white arrow on the SEM image. An example of a pale stripe in the SEM and a corresponding dark line in the CL map running parallel to the miscut are highlighted by yellow arrows. In a previous study,⁹ the elongated surface features and pale stripes have been identified as individual $\{111\}$ SFs or SF bunches intersecting the (001) surface along the $\langle 110 \rangle$ directions. The reduced CL intensity at these defects has been associated with non-radiative recombination centers, and one suggestion for the mechanism of non-radiative recombination relates to an enrichment of point defects in the vicinity of SFs.

The mean spectrum across the CL map shown in Fig. 1(b) is given in Fig. 1(c), which was generated by averaging the point spectra across all pixels in the hyperspectral CL maps. At least four different peaks can be identified, which are marked by arrows, indicating peak 1 to peak 4 from high to low energy. The peak energies were determined by a multiple-Gaussian fit of the mean spectrum, and are about 3.23, 3.15, 3.02, and 2.92 eV, from peak 1 to peak 4, respectively. (The CL mean spectra of a Mg-doped sample and a non-intentionally doped zb-GaN sample are compared in Fig. S1 in the supplementary material.) To identify the possible recombination mechanisms leading to those peaks, we have correlated our measurement results with literature on the luminescence properties of zb-GaN:Mg. Powell *et al.* and Xu *et al.* have both identified characteristic peaks in the photoluminescence (PL) spectra of zb-GaN:

24 June 2025 15:00:39



24 June 2025 15:00:39

FIG. 1. (a) SE image, (b) the corresponding panchromatic CL map, and (c) the mean spectrum of the CL map for the zb-GaN:Mg sample. The red dashed rectangle, white arrow, and yellow arrow indicate a rectangular feature, a surface feature, and a pale stripe in the SE image, and their corresponding optical behaviors in the CL map. The four arrows in the mean spectrum in (c) indicate peak 1 to peak 4 from high to low energy.

Mg thin films and discussed the possible recombination mechanisms of those peaks.^{13,24} Based on their studies, we attribute peak 1 in the CL mean spectrum [Fig. 1(c)] to be an excitonic transition, while peak 2 might be the near band edge donor-to-acceptor transition (NBE-DAP) at about 3.15 eV, which involves very shallow Mg acceptors.^{13,24} Peak 3 may be related to another DAP transition

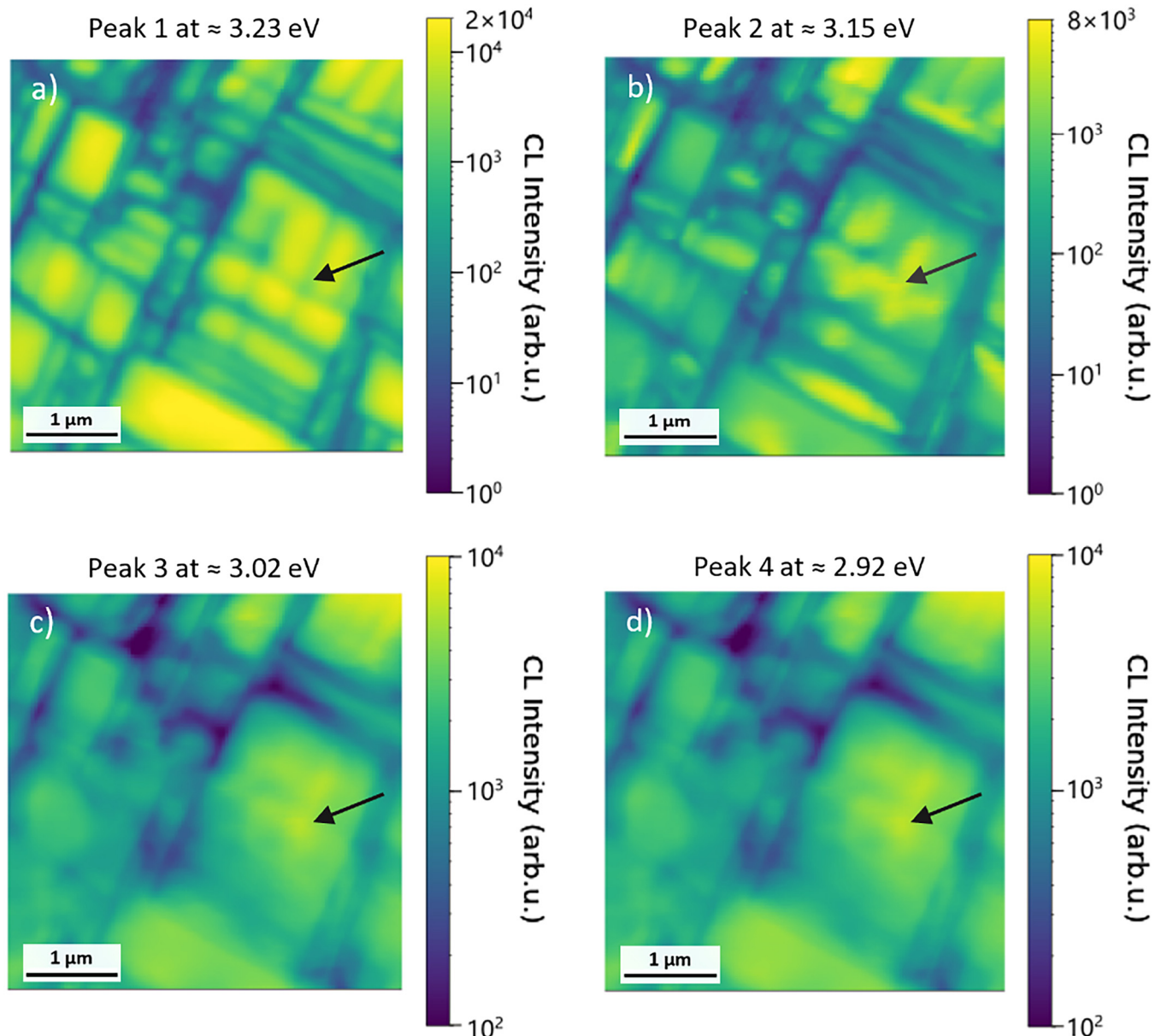
involving shallow Mg acceptors, of which the energy level is deeper from that for the NBE-DAP transition of peak 2.^{13,14} Peak 4 has been previously identified as blue band luminescence (BL).^{24,25} The cause of BL is not well understood though some attribute it to the DAP transition from a deep donor to a shallow Mg acceptor, where the donor may be a nitrogen vacancy/Mg acceptor complex.^{13,26} As

peak 2, peak 3, and peak 4 are all suggested to relate to Mg, the spatial distributions of their emissions should provide direct information on the location of Mg dopants in the sample.

To investigate the spatial distribution of CL emission from the characteristic peaks in the mean spectrum, bandpass filters have been applied, which show the CL emission intensity that lies within a selected energy range. These energy ranges were determined by

the full-width-half-maximum (FWHM) of each individual peak, after fitting the mean spectrum with multiple Gaussians.

The bandpass filtered CL intensity maps in Figs. 2(a)–2(d) show the spatial distribution of peak 1–4, respectively. The high-intensity areas for peak 1 in Fig. 2(a) are mainly located on the flat rectangular features previously observed in the SE image [see Fig. 1(a)]. Meanwhile, the dark stripes with low emission intensity



24 June 2025 15:00:39

FIG. 2. Bandpass filtered CL intensity maps of zb-GaN:Mg illustrating the distributions of (a) peak 1 at ≈ 3.23 eV, (b) peak 2 at ≈ 3.15 eV, (c) peak 3 at ≈ 3.02 eV, and (d) peak 4 at ≈ 2.92 eV. The intensity for each map is in the log-scale. The black arrows show one example area that is dark in 2(a) but bright in 2(b)–2(d).

for peak 1 are associated with the surface features or the pale stripes, which are both SF-related. This is consistent with the suggestion above that non-radiative recombination occurs at or near the SFs in zb-GaN.

The spatial distribution of peak 2 in Fig. 2(b) is different from that of peak 1. Most of the peak 2 intensity comes not only from areas with rectangular features but also from some of the regions that are on or close to SFs. Though some of the dark lines in Fig. 2(a) match the dark lines in the other three maps, some narrow dark lines in Fig. 2(a) correspond to the high-intensity lines in other maps. An example is marked by the black arrows in Fig. 2: the two intersecting dark lines in Fig. 2(a) correspond to the bright, high-intensity crossing in Fig. 2(b). Fainter and less sharp but still discernible bright features can also be seen in Figs. 2(c) and 2(d). These local differences may imply different recombination mechanisms for peak 1 from all other peaks (2, 3, and 4), consistent with our interpretation of the peak origins.

To compare the relative intensities of peaks 2 to 4 to that of peak 1 at the SF locations, ratios were determined from the bandpass filtered intensity maps for peaks 2, 3, and 4 to the peak 1 map, respectively. The ratio map from peak 2 to peak 1 is shown in Fig. 3(a). A ratio greater than 1 means that peak 2 has a higher intensity than peak 1 at the same position. The figure shows that the areas with ratio <1 are mainly on the rectangular features, while the areas with ratio >1 are on or near the SF-related features, which are at the edge of the rectangular features. This result shows that peak 2 is stronger compared to peak 1 at SF locations, and the ratio map depicts this in a clearer way, which matches the distribution of features related to SFs in the SE image [see Fig. 1(a)]. The observation may suggest that the Mg acceptors involved in peak 2 DAP transition tend to segregate toward SFs. Similar results were found in the ratio maps for peaks 3 and 4, as shown in Figs. 3(b) and 3(c). In the ratio maps for peaks 3 and 4, the ratio >1 areas are mainly on or close to SFs. The ratio map for peak 3 is darker than the peak 4 map, consistent with the fact that peak 3 is weaker than peak 4 in the mean spectrum [Fig. 1(c)]. This might indicate that different numbers of the acceptors or donors are involved in the recombination process for peaks 3 and 4, or that the lifetime differences between the different transitions and transfer of carriers between them impact their intensities. The analysis for peaks 3 and 4 may also suggest the segregation of Mg acceptors toward SFs, though peak 2, peak 3, and 4 may involve Mg acceptors with different energy levels.

The point spectra on and away from SF locations also provide an opportunity to compare the intensities of different peaks. Figure 4(a) is the bandpass-filter image for peak 1 marked with locations from which point spectra have been taken. Point spectra A and B were extracted from the center of bright rectangular regions away from SFs as marked in Fig. 4(a). In these point spectra, the excitonic peak has a higher intensity and is more dominant than the others, while peak 2 has a very low intensity, slightly above the background level. In the point spectra C and D taken at SF locations, the intensity of peak 1 is greatly reduced while that of peak 2 is increased. This may suggest more Mg acceptors being present in the vicinity of SFs than in the defect-free rectangular areas, which also supports our suggestion of Mg segregation at or near SFs.

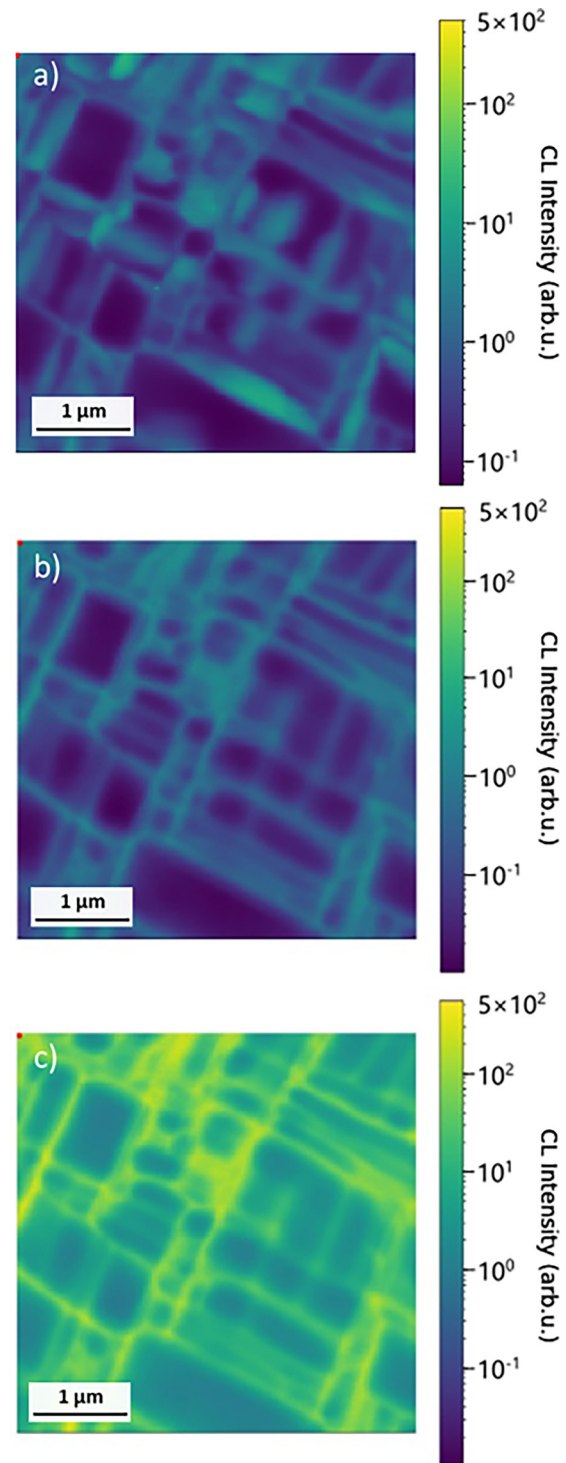


FIG. 3. CL distribution maps of zb-GaN:Mg showing the intensity ratio of (a) peak 2, (b) peak 3, and (c) peak 4 to the intensity of peak 1. The ratios are all in the log-scale.

24 June 2025 15:00:39

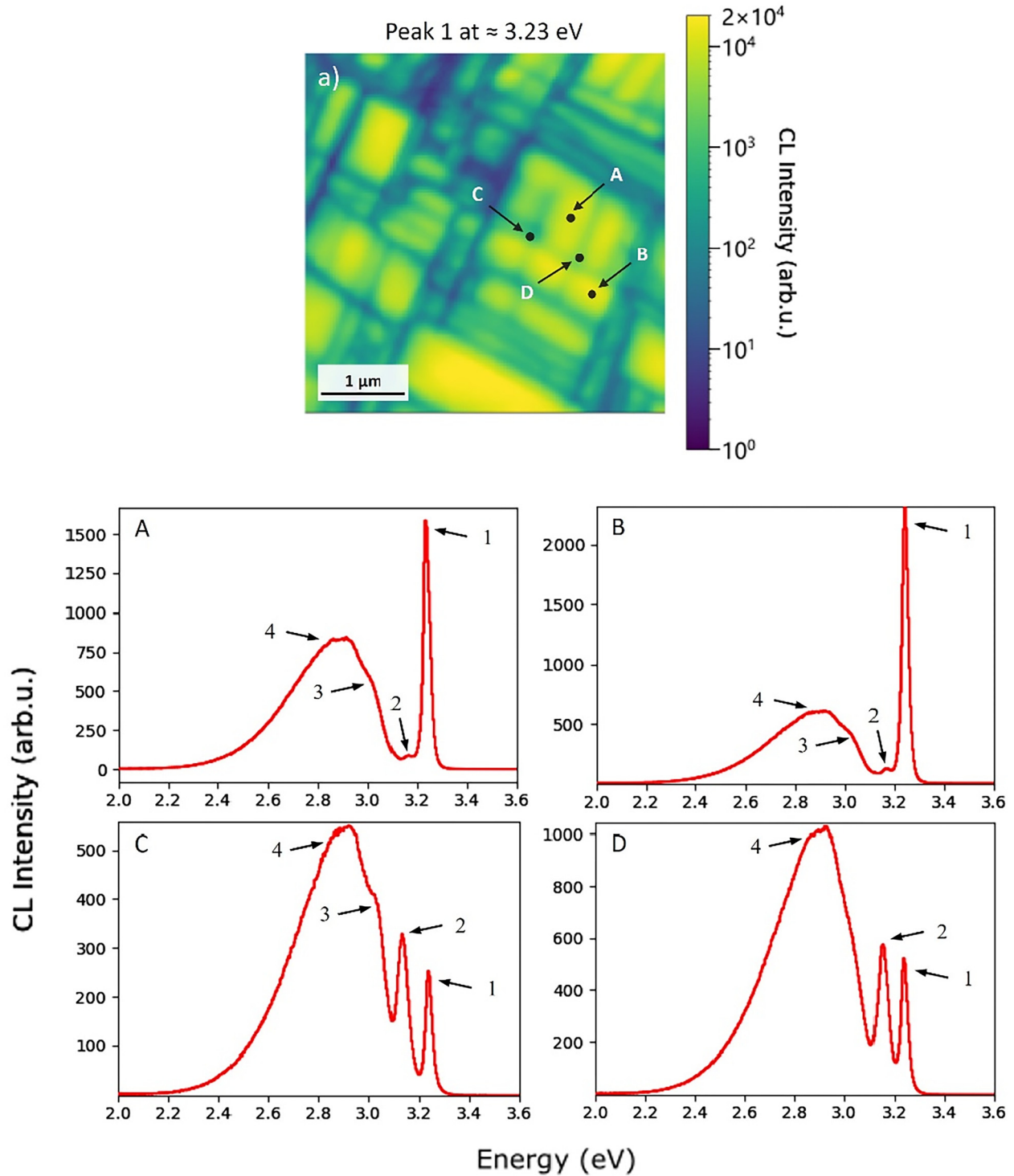


FIG. 4. CL point spectra at and away from the SF locations in zb-GaN:Mg. (a) is the bandpass-filter map at 3.23 eV, to show SF locations. Four points were chosen: points A and B are away from SFs and point C and D are at the SF locations. Point spectra A, B, C, and D were extracted from points A, B, C, and D, respectively. Peaks 1–4 are marked by black arrows.

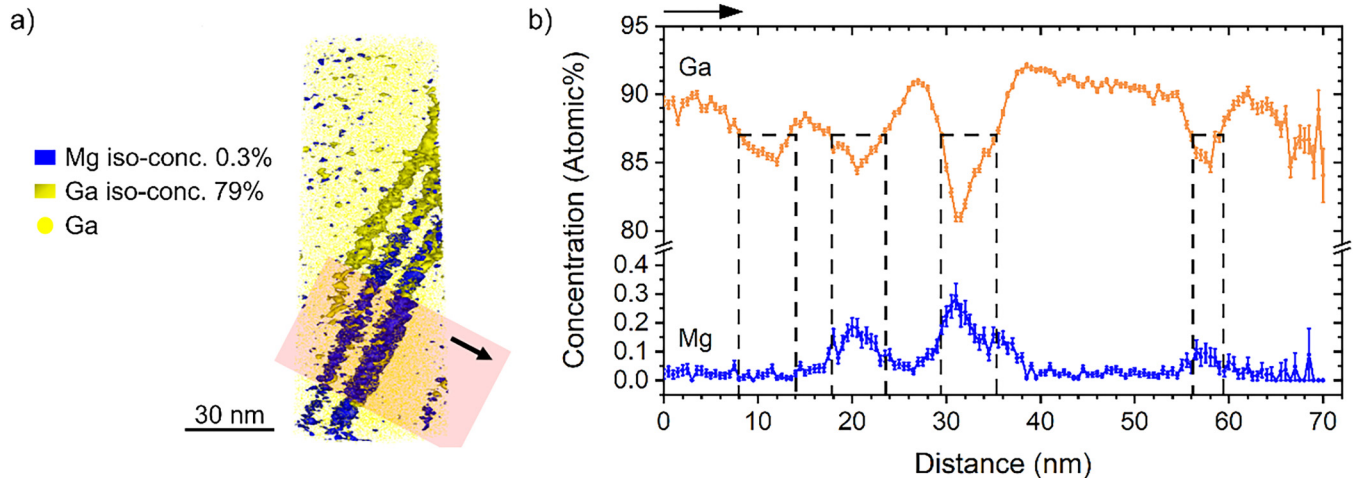


FIG. 5. (a) APT reconstruction highlighting the stacking fault region with Ga isoconcentration surface at 79% and Mg iso-concentration surface at 0.3% of the zb-GaN:Mg epilayer. Ga atoms are shown in yellow. (b) The 1D concentration profile taken along the direction indicated by the black arrow in (a). The red box region measures $40 \times 40 \times 70 \text{ nm}^3$. The SF regions are highlighted by black dashed boxes.

To seek for further evidence of Mg segregation toward SFs, we performed APT on a similar zb-GaN:Mg sample. Figure 5(a) shows an APT reconstruction in which Ga and Mg iso-concentration surfaces highlight planar features inclined at an approximately 60° angle to the horizontal. For this sample, due to the 4° miscut of the pseudo-substrate, stacking faults running parallel to the miscut direction are inclined at 55° to the GaN/SiC interface, while stacking faults running perpendicular to the miscut direction are inclined at 51° or 59° to the GaN/SiC interface in order to accommodate the miscut.⁷ Hence, the approximate angle of the features observed in APT is consistent with the expected angle of some of the SFs. Furthermore, recent APT studies of zb-GaN have provided evidence for biased evaporation at SFs. Structural changes at the SF lead to a locally higher field, which enhances the N detection rate, leading to the appearance of Ga depletion at or near the SF.²⁷ 1D concentration profiles were taken along the direction indicated by the black arrow in Fig. 5(a). The profiles are shown in Fig. 5(b), with the black dashed boxes indicating the positions of the inclined features shown in Fig. 5(a). This shows that the yellow Ga isoconcentration surfaces in Fig. 5(a) correspond to regions of reduced Ga content, as has previously been attributed to the presence of SFs. The Mg concentration was found to increase in some of these regions identified to be associated with SFs. This enrichment of Mg suggests that some amount of Mg segregate toward or onto the SFs. Taken together, the CL results and the APT results support the suggestion that Mg acceptors are involved in the mechanisms of the emission of light from these samples at 3.15, 3.02, and 2.92 eV (peaks 2, 3, and 4) and that these Mg acceptors segregate to SFs.

IV. SUMMARY

In summary, the relationship between Mg distribution and SFs in zb-GaN:Mg was investigated by CL and APT. Four emission

peaks were identified, with the highest energy peak attributed to excitonic transitions while the remaining peaks are consistent with Mg-related DAP transitions. SFs can be identified by a drop in the emission associated with the excitonic transition, but at the SF locations, the Mg-related DAP transitions can sometimes be brighter than in the SF-free regions. Even where CL maps of the DAP transitions show reduced intensity at the SF locations, the drop in intensity is not as large as the drop in intensity of the excitonic emission (i.e., the Mg-related DAP emissions are always relatively high at the SF). This led to the suggestion that Mg may segregate toward SFs, which is supported by APT measurements that indicate Mg rich planes through zb-GaN:Mg at an angle consistent with the SF orientation and adjacent to regions of apparent Ga depletion, which have previously been associated with SFs.

SUPPLEMENTARY MATERIAL

The supplementary material shows two cathodoluminescence spectra of a zb-GaN:Mg sample and a NID zb-GaN sample to illustrate the Mg-related optical transitions.

ACKNOWLEDGMENTS

This work was enabled through financial support by the UK Engineering and Physical Sciences Research Council (EPSRC) under Research Grant No. EP/W03557X/1, "Fast Switching Zincblende GaN LEDs" and No. EP/Y004213/1, "Segregation of alloy and dopant atoms at defects in nitride materials." The CL facility was funded by the EPSRC Grant No. EP/R025193/1, "Time-resolved cathodoluminescence scanning electron microscope." The APT characterization was funded by EPSRC under Grant No. EP/S021663/1: "A LEAP 5000 XS for the UK National Atom Probe Facility." The authors acknowledge the use of characterization facilities within the David Cockayne Centre for Electron

24 June 2025 15:00:39

Microscopy, Department of Materials, University of Oxford, alongside the financial support provided by the Henry Royce Institute under Grant No. EP/R010145/1. For the purpose of Open Access, the author has applied a CC BY public copyright license to any Author Accepted Manuscript (AAM) version arising from this submission.

AUTHOR DECLARATIONS

Conflict of Interest

The authors have no conflicts to disclose.

Author Contributions

Xiuyuan Xu: Data curation (equal); Formal analysis (equal); Visualization (equal); Writing – original draft (equal); Writing – review & editing (equal). **Martin Frentrup:** Conceptualization (equal); Methodology (equal); Supervision (equal); Visualization (equal); Writing – review & editing (equal). **Gunnar Kusch:** Data curation (equal); Supervision (equal); Writing – review & editing (equal). **Ruiying Shu:** Data curation (equal); Formal analysis (equal); Visualization (equal); Writing – review & editing (equal). **Christina Hofer:** Formal analysis (equal); Supervision (equal); Visualization (equal); Writing – review & editing (equal). **Paul A. J. Bagot:** Formal analysis (equal); Supervision (equal); Writing – review & editing (equal). **Michael P. Moody:** Formal analysis (equal); Funding acquisition (equal); Supervision (equal); Writing – review & editing (equal). **Menno J. Kappers:** Investigation (equal); Writing – review & editing (equal). **David J. Wallis:** Funding acquisition (equal); Supervision (equal); Writing – review & editing (equal). **Rachel A. Oliver:** Conceptualization (equal); Formal analysis (equal); Funding acquisition (equal); Methodology (equal); Project administration (lead); Supervision (equal); Writing – original draft (equal); Writing – review & editing (equal).

DATA AVAILABILITY

The data that support the findings of this study are openly available in the University of Cambridge repository Apollo at <https://doi.org/10.17863/CAM.118949>, Ref. 28.

REFERENCES

- ¹C. Zhou, A. Ghods, V. G. Saravade, P. V. Patel, K. L. Yungchans, C. Ferguson, Y. Feng, B. Kucukgok, N. Lu, and I. T. Ferguson, “Review—The current and emerging applications of the III-nitrides,” *ECS J. Solid State Sci. Technol.* **6**(12), Q149–Q156 (2017).
- ²Y. Wu, X. Liu, A. Pandey, P. Zhou, W. J. Dong, P. Wang, J. Min, P. Deotare, M. Kira, E. Kioupakis, and Z. Mi, “III-nitride nanostructures: Emerging applications for micro-LEDs, ultraviolet photonics, quantum optoelectronics, and artificial photosynthesis,” *Prog. Quantum Electron.* **85**, 100401 (2022).
- ³G. Verzellesi, D. Saguatti, M. Meneghini, F. Bertazzi, M. Goano, G. Meneghesso, and E. Zanoni, “Efficiency droop in InGaN/GaN blue light-emitting diodes: Physical mechanisms and remedies,” *J. Appl. Phys.* **114**(7), 071101 (2013).
- ⁴C. X. Ren, “Polarisation fields in III-nitrides: Effects and control,” *Mater. Sci. Technol.* **32**(5), 418–433 (2016).

- ⁵M. Monavarian, A. Rashidi, and D. Feezell, “A decade of nonpolar and semipolar III-nitrides: A review of successes and challenges,” *Phys. Status Solidi A* **216**, 1800628 (2018).
- ⁶Y.-C. Tsai, J.-P. Leburton, and C. Bayram, “Quenching of the efficiency droop in cubic phase InGaAlN light-emitting diodes,” *IEEE Trans. Electron Devices* **69**(6), 3240–3245 (2022).
- ⁷L. Y. Lee, M. Frentrup, P. Vacek, M. J. Kappers, D. J. Wallis, and R. A. Oliver, “Investigation of stacking faults in MOVPE-grown zincblende GaN by XRD and TEM,” *J. Appl. Phys.* **125**(10), 105303 (2019).
- ⁸S. A. Church, S. Hammersley, P. W. Mitchell, M. J. Kappers, S. L. Sahonta, M. Frentrup, D. Nilsson, P. J. Ward, L. J. Shaw, D. J. Wallis, C. J. Humphreys, R. A. Oliver, D. J. Binks, and P. Dawson, “Photoluminescence studies of cubic GaN epilayers,” *Phys. Status Solidi B* **254**(8), 1600733 (2017).
- ⁹A. Gundimeda, G. Kusch, M. Frentrup, M. J. Kappers, D. J. Wallis, and R. A. Oliver, “Cathodoluminescence studies of the optical properties of a zincblende InGaN/GaN single quantum well,” *Nanotechnology* **35**(39), 395705 (2024).
- ¹⁰N. Izyumskaya, N. Izyumskaya, F. Zhang, S. Okur, T. Selden, V. Avrutin, Ü. Özgür, S. Metzner, C. Karbaum, F. Bertram, J. Christen, and H. Morkoç, “Optical studies of strain and defect distribution in semipolar (1101) GaN on patterned Si substrates,” *J. Appl. Phys.* **114**(11), 113502 (2013).
- ¹¹S. Okur, S. Metzner, N. Izyumskaya, F. Zhang, V. Avrutin, C. Karbaum, F. Bertram, J. Christen, H. Morkoç, and Ü. Özgür, “Microscopic distribution of extended defects and blockage of threading dislocations by stacking faults in semipolar (11 $\bar{0}$ 1) GaN revealed from spatially resolved luminescence,” *Appl. Phys. Lett.* **103**(21), 211908 (2013).
- ¹²T. M. Schmidt, R. H. Miwa, W. Orellana, and H. Chacham, “Stacking fault effects in Mg-doped GaN,” *Phys. Rev. B* **65**(3), 1–4 (2002).
- ¹³R. E. L. Powell, S. V. Novikov, C. T. Foxon, A. V. Akimov, and A. J. Kent, “Photoluminescence of magnesium and silicon doped cubic GaN,” *Phys. Status Solidi C* **11**(3–4), 385–388 (2014).
- ¹⁴D. J. As, T. Simonsmeier, B. Schöttker, T. Frey, D. Schikora, W. Kriegseis, W. Burkhardt, and B. K. Meyer, “Incorporation and optical properties of magnesium in cubic GaN epilayers grown by molecular beam epitaxy,” *Appl. Phys. Lett.* **73**(13), 1835–1837 (1998).
- ¹⁵B. Monemar, P. P. Paskov, G. Pozina, C. Hemmingsson, J. P. Bergman, S. Khromov, V. N. Izyumskaya, V. Avrutin, X. Li, H. Morkoç, H. Amano, M. Iwaya, and I. Akasaki, “Properties of the main Mg-related acceptors in GaN from optical and structural studies,” *J. Appl. Phys.* **115**(5), 053507 (2014).
- ¹⁶J. Lähnemann, U. Jahn, O. Brandt, T. Flissikowski, P. Dogan, and H. T. Grahn, “Luminescence associated with stacking faults in GaN,” *J. Phys. D: Appl. Phys.* **47**, 423001 (2014).
- ¹⁷A. Gundimeda, G. Kusch, M. Frentrup, H. Xiu, R. Shu, C. Hofer, P. A. J. Bagot, M. P. Moody, M. J. Kappers, D. J. Wallis, and R. A. Oliver, “Impact of stacking faults on the luminescence of a zincblende InGaN/GaN single quantum well,” *J. Phys. D: Appl. Phys.* **58**(2), 025112 (2025).
- ¹⁸A. Kumar, J. Uzuhashi, T. Ohkubo, R. Tanaka, S. Takashima, M. Edo, and K. Hono, “Atomic-scale quantitative analysis of implanted Mg in annealed GaN layers on free-standing GaN substrates,” *J. Appl. Phys.* **126**(23), 235704 (2019).
- ¹⁹A. Kumar, W. Yi, T. Ohkubo, J. Chen, T. Sekiguchi, R. Tanaka, S. Takashima, M. Edo, and K. Hono, “Impact of high-temperature Mg-implantation on defects and dopants distribution in GaN,” *J. Appl. Phys.* **133**(18), 185702 (2023).
- ²⁰L. Y. Lee, M. Frentrup, M. J. Kappers, R. A. Oliver, C. J. Humphreys, and D. J. Wallis, “Effect of growth temperature and V/III-ratio on the surface morphology of MOVPE-grown cubic zincblende GaN,” *J. Appl. Phys.* **124**(10), 105302 (2018).
- ²¹T. J. Wade, A. Gundimeda, M. J. Kappers, M. Frentrup, S. M. Fairclough, D. J. Wallis, and R. A. Oliver, “MOVPE studies of zincblende GaN on 3C-SiC/Si (001),” *J. Cryst. Growth* **611**, 127182 (2023).

- ²²J. Lähnemann, J. Ferrer Orri, E. Prestat, H. W. Ånes, D. N. Johnstone, L. G. T. M. Migrator, and N. Tappy, *LumiSpy/Lumispy: v0.2.2 (v0.2.2)* (Zenodo, 2023).
- ²³K. Thompson, D. Lawrence, D. J. Larson, J. D. Olson, T. F. Kelly, and B. Gorman, “*In situ* site-specific specimen preparation for atom probe tomography,” *Ultramicroscopy* **107**(2–3), 131–139 (2007).
- ²⁴D. Xu, H. Yang, D. G. Zhao, S. F. Li, and R. H. Wu, “Room-temperature optical transitions in Mg-doped cubic GaN/GaAs (100) grown by metalorganic chemical vapor deposition,” *J. Appl. Phys.* **87**(4), 2064–2066 (2000).
- ²⁵E. Martinez-Guerrero, B. Daudin, G. Feuillet, H. Mariette, Y. Genuist, S. Fanget, A. Philippe, C. Dubois, C. Bru-Chevallier, G. Guillot, P. A. Nze, T. Chassagne, Y. Monteil, H. Gamez-Cuatzin, and J. Tardy, “P and n type doping of cubic GaN on SiC (001),” *Mater. Sci. Eng. B* **82**(1–3), 59–61 (2001).
- ²⁶Y. Hu, C. A. Hernández-Gutiérrez, H. I. Solís-Cisneros, G. Santana, Y. Kudriatsev, J. L. Camas-Anzueto, and M. López-López, “Blue luminescence origin and Mg acceptor saturation in highly doped zinc-blende GaN with Mg,” *J. Alloys Compd.* **897**, 163133 (2022).
- ²⁷R. Shu, R. A. Oliver, M. Frentrup, M. J. Kappers, H. Xiu, G. Kusch, D. J. Wallis, C. Hofer, P. A. J. Bagot, and M. P. Moody, “Beyond TEM imaging: Atom probe tomography reveals chemical inhomogeneity at stacking fault interfaces in InGaN/GaN LEDs,” *Materialia* **40**, 102417 (2025).
- ²⁸X. Xu, M. Frentrup, G. Kusch, R. Shu, C. Hofer, P. A. J. Bagot, M. P. Moody, M. J. Kappers, D. J. Wallis, and R. A. Oliver, “Research data supporting 'Point defect luminescence associated with stacking faults in magnesium doped zinc-blende GaN,'” Apollo Repository (University of Cambridge, 2025), available at <https://doi.org/10.17863/CAM.118949>